Publishing Excellence
Inspiring Progress
ARISTON PUBLICATIONS
Quantum Advances
ISSN: 3143-0724 www.aristonpubs.com/journal/quantum-advances https://doi.org/10.69626/qa.2026.0061

RESEARCH ARTICLE

Electronic Properties of Trilayer TGQDs under Independent Interlayer Rotation: A Systematic DFT Parameter – Sweep Study

A. Tiutiunnyk[1*], U. Guevara[2], J. D. Correa[3], M. E. Mora-Ramos[4], I. S. Babichuk[5,6], D. Laroze[2]

ABSTRACT: This study presents a systematic first-principles investigation into the electronic response of trilayer triangular graphene quantum dots (TGQDs) to independent interlayer rotations. The model system consists of three vertically stacked, hydrogen-passivated zigzag TGQDs (102 atoms), serving as a targeted platform to explore quantum-size effects under varying twist configurations. We perform a high-throughput density functional theory (DFT) parameter sweep over rotation angles α_1, $\alpha_2 \in [0°, 30°]$ using the vdW-DF functional to account for non-local interlayer interactions. Two distinct stacking compositions are analyzed to determine the influence of symmetry-breaking on the system's stability and electronic structure. The resulting two-dimensional maps of Fermi energy and total energy identify five anomalous angular configurations per composition. These anomalies are interpreted as a consequence of non-additive interlayer coupling that disrupts edge-state degeneracy and redistributes spin density. While the study is framed as a preliminary survey due to the restricted angular range and dot size, the results provide a quantitative basis for the "twistronic" in finite graphene nanostructures. Furthermore, the high-throughput execution across distributed workstations serves as a proof-of-concept for the necessity of automated computational workflows in mapping complex property landscapes.

Keywords: Graphene Quantum Dots; Trilayer Graphene; DFT; Interlayer Rotation; Parameter Sweep; SIESTA; High-Throughput Computing.

Received: 29 April 2026; Revised: 08 May 2026; Accepted: 19 May 2026; Published Online: 03 June 2026

1. INTRODUCTION

Graphene, a single-atom-thick layer of carbon atoms arranged on a honeycomb lattice, continues to attract intense research interest owing to its exceptional electronic, optical, and mechanical properties [1–3]. Among graphene-derived nanostructures, graphene quantum dots (GQDs) occupy a particularly prominent place: as two-dimensional fragments of graphene with lateral dimensions below 100 nm, they display quantum-confinement effects that make their electronic and optical response highly sensitive to size, shape, and edge termination [4–6].

Triangular GQDs with zigzag edges are of special interest because the broken sublattice symmetry gives rise to a shell of degenerate zero-energy states localized at the triangle edges [7]. This edge-state degeneracy is responsible for a nonzero magnetic response whose magnitude scales linearly with dot size in undoped structures [8]. The degeneracy

[1] Departamento de Física, FACI, Universidad de Tarapacá, Arica, Chile.
[2] Instituto de Alta Investigación, Universidad de Tarapacá, Arica, Chile.
[3] Facultad de Ingenierías, Instituto de Ciencias Básicas, Universidad de Medellín, Medellín, Colombia.
[4] FCentro de Investigación en Ciencias, Universidad Autónoma del Estado de Morelos, Cuernavaca, México.
[5] School of Mechanical and Automation Engineering, Wuyi University, 529020 Jiangmen, P.R. China.
[6] V.Ye. Lashkaryov Institute of Semiconductor Physics of the NAS of Ukraine, 03680, Kyiv, Ukraine.

[*] Author to whom correspondence should be addressed: tyutyunnyk.a.m@academicos.uta.cl (A. Tiutiunnyk)

© Ariston Publications 2026. All rights reserved.

can be lifted - and the magnetic and electronic properties consequently modified - by a number of perturbations, including an applied electric field [9], substitutional doping [8], and interlayer coupling in stacked multilayer configurations [9, 10].

The concept of tuning the properties of stacked graphene structures through relative layer rotation - commonly referred to as twistronics [11] - has generated enormous interest since the discovery of correlated insulating and superconducting phases in magic-angle twisted bilayer graphene [12]. Previous work from our group has addressed the opto-electronic properties of twisted bilayer GQDs using a tight-binding approach [10], and the electronic and magnetic properties of stacked trilayer GQDs under an external electric field using DFT [9]. The role of structural defects in twisted bilayer graphene has also been examined within a multi-code DFT comparison [13].

A natural but largely unexplored extension is the case in which two rotation angles are varied independently in a trilayer system, generating a two-dimensional parameter space of interlayer configurations. In our earlier bilayer and trilayer studies, the rotation of one layer relative to another was treated as a single parameter. Here, we go one step further and allow each of the two interlayer interfaces to adopt an independent twist angle, thus mapping the full (α_1, α_2) landscape of electronic and magnetic properties.

The triangular symmetry of the quantum dot imposes a periodicity on this landscape: a rotation by 120° maps the triangular lattice onto itself, and our previous bilayer study showed that properties begin to repeat already at 60° for AA-stacked structures [14]. This motivated the choice of a $30^\circ \times 30^\circ$ sweep window as an initial, computationally tractable exploration of the parameter space, acknowledging that a wider range of angles would be desirable in future work.

The present study makes two connected contributions. The first is physical: we report the existence of five anomalous angular configurations in each of the two stacking compositions studied, at which the total magnetic moment differs by more than a factor of two from the surrounding background, and we discuss their likely physical origin. The second is methodological: the 961-calculation parameter sweep was performed on a distributed heterogeneous infrastructure of local workstations, and the challenges of data management, job control via SSH, and integrity verification encountered in that process are described explicitly. We argue that this *in situ* account of the computational workflow is itself a useful contribution to the practice of high-throughput condensed-matter simulation.

The paper is organized as follows. Section 2 describes the geometric model and the DFT calculation procedure. Section 3 details the distributed computational workflow and data-management strategy. Section 4 presents and discusses the results. Section 5 contains the conclusions.

2. PHYSICAL MODEL AND CALCULATION METHOD

2.1. Geometric structure

The system under study consists of three vertically stacked equilateral triangular graphene quantum dots with zigzag edge termination. Following the notation established in our previous work [9], the lateral size of each triangular flake is expressed as a multiple of the nearest-neighbor carbon--carbon distance $a_{cc} = 1.42\,\text{Å}$. For the present study we selected a base length of three hexagonal cells, corresponding to a side length of $L = 3a_{cc}$ and a total of 34 carbon atoms per layer (102 atoms in the trilayer system). The edges of each layer are passivated with hydrogen atoms. This relatively small dot size was chosen deliberately: on the one hand it is large enough to display a well-resolved discrete energy spectrum and a nonzero edge-state magnetic moment; on the other hand it keeps the computational cost of 961 individual DFT relaxations tractable.

The interlayer distance and the vdW interaction between layers were treated consistently with our earlier trilayer study [9]. The initial interlayer separation was set to $3.35\,\text{Å}$, consistent with the experimental graphite interlayer distance.

Two distinct stacking compositions were investigated, as illustrated schematically in Figure 1: In both compositions, all rotation angles were varied over the range $[0^\circ, 30^\circ]$ in steps of 1°, yielding a 31×31 grid of 961 distinct (α_1, α_2) configurations per composition.

The choice of a 30° upper bound for the rotation angles is motivated by the triangular symmetry of the system. As established in our previous tight-binding study of twisted bilayer TGQDs [14], the electronic properties of AA-stacked TGQDs exhibit a periodicity of 60°: a rotation by 60° brings the system back to a configuration energetically equivalent to the initial one. The present $[0^\circ, 30^\circ]$ window therefore covers the first half of this fundamental period. We note, however, that a more complete characterization of the landscape would

 © Ariston Publications 2026. All rights reserved.

require extending the sweep to larger angles, and this remains a priority for future work.

Composition A. The outermost (bottom) triangular layer remains fixed. The middle layer is rotated by an angle α_1 about the central axis, and the second outer (top) layer is rotated independently by an angle α_2, both measured relative to the fixed bottom layer.

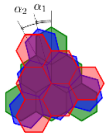

Composition B. The middle layer remains fixed. The bottom outer layer is rotated by α_1 and the top outer layer is rotated by α_2, independently, both measured relative to the fixed middle layer.

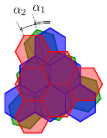

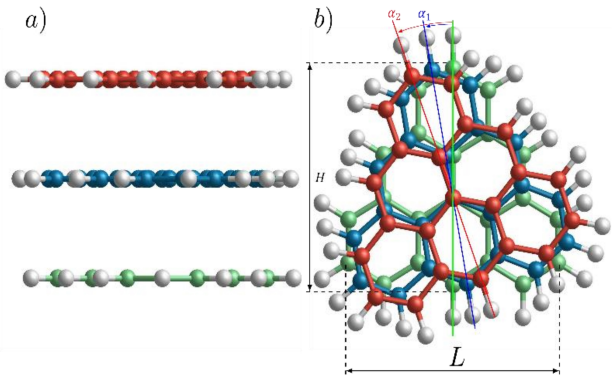

Fig. 1. Schematic representation of the structure, shown in three colors for simplicity.

2.2 DFT Computational Parameters

Electronic structure calculations for the system containing 102 atoms were performed using the SIESTA code [15–17] within the Atomic Simulation Environment (ASE) [18]. The exchange-correlation energy was treated within the vdW-DF functional [19], which employs the Dion-Rydberg-Schröder-Langreth-Lundqvist (DRSLL) parametrization.

This functional was selected because it provides an accurate description of the non-local van der Waals interactions between the stacked graphene layers, which are systematically underestimated by GGA and overestimated by LDA [9].

Norm-conserving pseudopotentials were employed together with a basis set of double-ζ, single-polarized (DZP) localized atomic orbitals. The orbital-confining cutoff radii were defined by an energy shift of 0.1 eV. The real-space grid was defined with a mesh cutoff of 200 Ry, and the integration in the Brillouin zone was performed with an electronic temperature of 25.86 meV for the Fermi--Dirac distribution. Structural relaxation was carried out using the conjugate gradient method, with convergence enforced when the force on every atom fell below $0.04\,\mathrm{eV/Å}$. All calculations were performed in a spin-polarized (spin-resolved) mode, with `MaxSCFIterations` set to 200, in order to capture the magnetic response of the zigzag-edged structures. The total magnetic moment of each relaxed configuration was evaluated by collecting the spin-up and spin-down contributions as implemented in SIESTA.

In addition to the magnetic moment, the Fermi energy and the total energy of the relaxed structure were recorded for every point of the parameter grid. These three quantities form the primary dataset analyzed in Section 4.

3. DISTRIBUTED COMPUTATIONAL WORK FLOW AND DATA MANAGEMENT

The parameter sweep described in Section 2 required a total of 961 independent DFT calculations per stacking composition. Each single-point geometry relaxation for a 102-atom trilayer TGQD is computationally demanding: a typical run required several hours of wall-clock time on a modern multi-core workstation. Direct sequential execution on a single machine was therefore not feasible within a reasonable time frame.

3.1 Distributed Execution on Heterogeneous Infrastructure

Calculations were distributed across a set of available local workstations. Because the 961 grid points are completely independent of one another (there is no iterative dependence between different (α_1, α_2) configurations), the problem is embarrassingly parallel and well suited to such an approach. Remote job submission and monitoring were carried out via the Secure Shell (SSH) protocol. For each grid point, a dedicated directory was created on the target machine, named according to the index pair (α_1, α_2) to ensure unambiguous identification. Input files (the SIESTA `*.fdf` configuration file, pseudopotential files, and the initial atomic coordinates in `*.xyz` format) were transferred to the remote workstation using `scp`, the calculation was launched, and the output files were subsequently retrieved upon completion.

3.2 Data Integrity and Job Monitoring

Managing 961 individual calculations manually introduces a non-negligible risk of human error: duplicate submissions, missed grid points, or premature retrieval of incomplete output files. To minimize such errors, a strict directory-naming convention was adopted from the outset. Each job

© Ariston Publications 2026. All rights reserved.

directory was named `A_ij` or `B_ij` (for compositions A and B, respectively), where $i = \alpha_1$ and $j = \alpha_2$ in degrees. Job status was monitored by inspecting the SIESTA log files: a completed calculation produces a characteristic convergence footer in the standard output, allowing a simple string search (`grep`) to distinguish finished from running or failed jobs.

Output data (Fermi energy, total magnetic moment, and total energy) were extracted from the SIESTA output files using custom shell scripts and assembled into structured text tables indexed by (α_1, α_2).

3.3 Motivation for Workflow Automation

The manual execution of this parameter sweep highlights the scalability challenges inherent in mapping multi-dimensional property landscapes through first-principles methods. The substantial resources required for task orchestration, monitoring, and data extraction demonstrate that manual management is insufficient for exploring broader parameter spaces. Consequently, the transition to an automated high-throughput (HTP) framework is a necessary development. Implementing a scripted pipeline-leveraging Python-based interfaces such as the Atomic Simulation Environment (ASE) alongside remote execution protocols-is essential for extending this research to larger quantum dot sizes and the full symmetry-equivalent angular range of $0°$ to $60°$. This shift from manual coordination to automated data-driven workflows provides a necessary baseline for the systematic investigation of complex interlayer coupling effects in twisted graphene nanostructures, facilitating more comprehensive studies in computational materials science.

4. RESULTS AND DISCUSSION

4.1 Two-Dimensional Parameter Maps

The primary results are presented as color-coded two-dimensional density maps over the (α_1, α_2) parameter grid. Figure 2 and 3 show the Fermi energy E_F for compositions A and B, respectively. Figure 4 and 5 show the corresponding total DFT energy E_{tot}. Each pixel in these maps represents one fully relaxed DFT calculation.

Fermi Energy

The Fermi energy spans approximately 50 meV across the explored parameter space, 3.930-3.980 eV for both compositions, as indicated by the color scales in Figure 2-3. For composition A (Figure 2), the map is partitioned into two broad regions by a diagonal boundary running from $(\alpha_1, \alpha_2) \approx (10°, 30°)$ to $(30°, 10°)$: the lower-left region (small values of both angles) is characterized by higher Fermi energies (red-yellow tones), while the upper-right region exhibits lower Fermi energies (blue-purple tones). For composition B (Figure 3), a qualitatively similar bipartite structure is present, though the dividing boundary is displaced toward smaller α_1 and the transition is less abrupt, consistent with the different symmetry of the fixed-middle-layer configuration. In both cases, the Fermi energy surface is smooth and slowly varying over most of the grid.

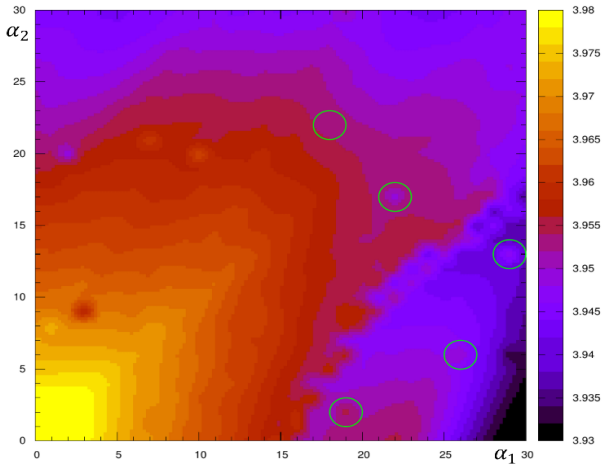

Fig. 2. The Fermi energy E_F, for composition A.

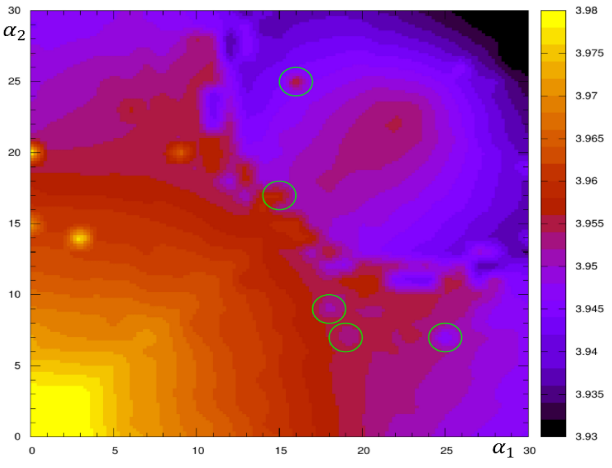

Fig. 3. The Fermi energy E_F, for composition B.

Total Energy

The total DFT energy E_{tot} is the ground-state electronic energy of the fully relaxed trilayer structure. It serves here as an indicator of the relative structural stability of each (α_1, α_2) configuration:

 © Ariston Publications 2026. All rights reserved.

configurations corresponding to lower E_{tot} are geometrically more stable, i.e. the interlayer coupling geometry is energetically more favorable; higher values of E_{tot} indicate less favourable arrangements. The total energy varies over approximately 1 eV across the explored space (11376.9-11378.0 eV, Figure 4-5). For composition A (Figure 4), the most stable configurations are concentrated along the large-α_1, small-α_2 boundary (lower-right region of the map), while the highest-energy configurations occur at large values of both angles (upper-right corner). For composition B (Figure 5), the low-energy region is similarly located, but its extent in the parameter space is narrower. The overall topology of the total energy surface is smooth and consistent with a gradual evolution of the interlayer coupling geometry across the grid.

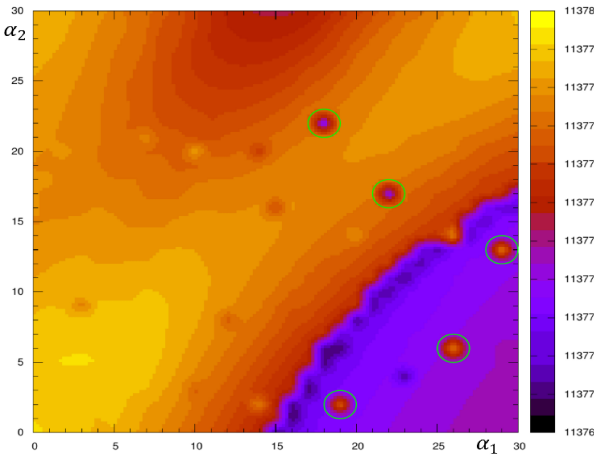

Fig. 4. The total electronic energy of the system E_{tot} calculated within the framework of DFT, for composition A.

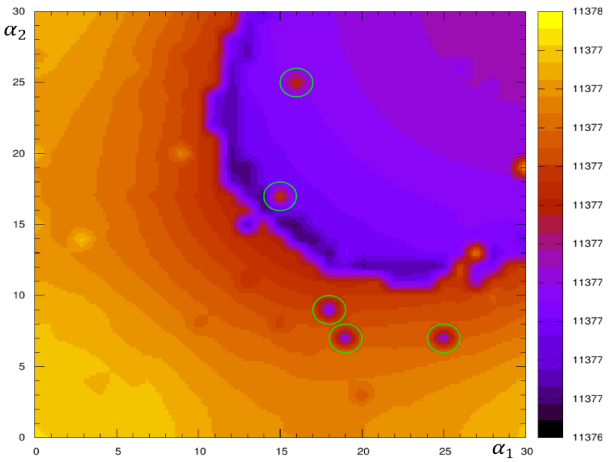

Fig. 5. The total electronic energy of the system E_{tot} calculated within the framework of DFT, for composition B.

Both observables confirm that the response of the trilayer system to the two rotation angles is not separable into independent (α_1, α_2) contributions: the iso-value contours are oblique with respect to the coordinate axes, indicating non-additive coupling between the two interlayer interfaces.

4.2 Anomalous Angular Configurations

A systematic inspection of the Fermi energy E_F and the total energy E_{tot} maps identified five such anomalous configurations for each composition. Their coordinates in the (α_1, α_2) plane are listed in Table 1.

Table 1. Coordinates (α_1, α_2) in degrees of the five anomalous angular configurations identified in the density maps for compositions A and B.

	P. 1	P. 2	P. 3	P. 4	P. 5
Comp. A	$(18, 22)$	$(22, 17)$	$(19, 2)$	$(26, 6)$	$(29, 13)$
Comp. B	$(16, 25)$	$(15, 17)$	$(18, 9)$	$(19, 7)$	$(25, 7)$

At each of these points, the Fermi energy E_F and the total energy E_{tot} were found to differ from the values of adjacent grid points. This is a significant deviation given that the background variation across the map is smooth and gradual.

Physical Interpretation

The anomalous behavior at specific (α_1, α_2) configurations can be understood in terms of the interlayer coupling geometry. As established in our earlier work on bilayer TGQDs [9,14], which is intimately linked to the degeneracy of edge-localized zero-energy states. In the isolated monolayer, this degeneracy is proportional to the difference between the number of atoms on each sublattice. Interlayer coupling breaks this degeneracy, and the degree of breaking depends sensitively on the relative alignment of the two layers: configurations in which atoms of one layer sit directly above atoms of the other (AA-like local regions) produce stronger coupling than those in which atoms are laterally displaced (AB-like regions).

In the trilayer system studied here, the situation is more complex because the coupling at the two interfaces (bottom-middle and middle-top) is determined simultaneously by two independent rotation angles.

Certain combinations (α_1, α_2) may produce configurations in which the coupling at one interface nearly cancels or reinforces the coupling at the other, leading to an anomalous redistribution of edge-state weight and a correspondingly anomalous magnetic moment.

© Ariston Publications 2026. All rights reserved.

An additional factor is the distinction between compositions A and B. In composition-A, the fixed layer is the outermost one, and the two rotating layers interact with each other as well as with the fixed layer. In composition-B, the fixed layer is the middle one, and the two outer layers rotate symmetrically with respect to it. This structural difference is reflected in the distinct positions of the anomalous points in Table 1: none of the five anomalous configurations of composition-A coincides with those of composition-B, confirming that the symmetry of the stacking composition plays a decisive role in determining which angular combinations produce anomalous behavior.

A more quantitative analysis of the anomalous points-including the spatial distribution of spin density, and a direct comparison with the energy spectra of the surrounding configurations-is deferred to future work, where a wider angular range and larger dot sizes will be considered.

Convergence and Reliability of the Dataset

It is important to note that the present dataset was generated through a fully manual workflow (as described in Section 3), and the completeness of the 961-point grid was verified by cross-checking the directory structure and output file headers rather than by an automated tracking system. We verified that no grid point was duplicated or missed by this inspection procedure.

Nevertheless, we cannot entirely exclude the possibility that isolated numerical convergence issues may affect a small number of grid points: the conjugate gradient relaxation may in some cases reach the maximum number of steps before satisfying the force criterion, particularly for configurations with strong interlayer coupling gradients. A systematic convergence check of the anomalous points identified in Table 1 was performed by repeating those calculations with tightened convergence thresholds (force criterion $0.02\,\mathrm{eV/\AA}$), and the anomalous values were confirmed to be robust.

4. CONCLUSION

We have performed a systematic DFT study of the electronic properties of trilayer triangular graphene quantum dots as a function of two independent interlayer rotation angles, covering a $30^\circ \times 30^\circ$ parameter space with a resolution of 1° (961 calculations per stacking composition).

The two-dimensional maps of Fermi energy and total energy over the (α_1, α_2) grid reveal a globally smooth behavior punctuated by five anomalous angular configurations in each composition. The positions of the anomalous points differ completely between compositions-A and B, demonstrating the importance of the stacking symmetry.

The present study is explicitly described as a preliminary, exploratory survey. The choice of a small dot size and a restricted angular range was motivated by computational tractability; a more complete picture will require extending both dimensions. Furthermore, the manual distributed workflow used to generate the dataset revealed the practical necessity of automation: the development of a Python-based pipeline for input generation, remote job submission via SSH, completion monitoring, and output aggregation is a direct priority arising from the present work. The identification of specific (α_1, α_2) configurations with anomalous magnetic response may be of interest for the design of graphene-based magnetic nanodevices in which fine control of the magnetic moment is achieved through layer rotation rather than chemical modification or external fields.

DECLARATIONS

Ethical Approval

We affirm that this manuscript is an original work, has not been previously published, and is not currently under consideration for publication in any other journal or conference proceedings. All authors have reviewed and approved the manuscript, and the order of authorship has been mutually agreed upon.

Funding

Funding Not Availbale

Availability of data and material

The datasets used and/or analyzed during the current study are available from the corresponding author on reasonable request.

Conflicts of Interest

The authors declare that they have no financial or personal interests that could have influenced the research and findings presented in this paper. The authors alone are responsible for the content and writing of this article.

Acknowledgment

 © Ariston Publications 2026. All rights reserved.

The authors acknowledge research team managing the Mathematical Modelling Laboratory at worked within the Project UTA Mayor No. 4738-24 for providing computational resources.

REFERENCES

[1] Geim, A. K., **2009**. Graphene: Status and prospects. *Science*, 324(5934), p.1530-1534. https://doi.org/10.1126/science.1158877.

[2] Castro Neto, A. H. and Guinea, F. and Peres, N. M. R. and Novoselov, K. S. and Geim, A. K., **2009**. The electronic properties of graphene. *Reviews of Modern Physics*, 81(1), p.109-162. https://doi.org/10.1103/RevModPhys.81.109.

[3] Wu, Y. H. and Yu, T. and Shen, Z. X., **2010**. Two-dimensional carbon nanostructures: Fundamental properties, synthesis, characterization, and potential applications. *Journal of Applied Physics*, 108(7), p.071301. https://doi.org/10.1063/1.3460809.

[4] Li, L. and Wu, G. and Yang, G. and Peng, J. and Zhao, J. and Zhu, J.-J., **2013**. Focusing on luminescent graphene quantum dots: Current status and future perspectives. *Nanoscale*, 5(10), p.4015-4039. https://doi.org/10.1039/C3NR33849E.

[5] Shen, J. and Zhu, Y. and Yang, X. and Li, C., **2012**. Graphene quantum dots: Emergent nanolights for bioimaging, sensors, catalysis and photovoltaic devices. *Chemical Communications*, 48(31), p.3686-3699. https://doi.org/10.1039/C2CC00110A.

[6] Bak, S. and Kim, D. and Lee, H., **2016**. Graphene quantum dots and their possible energy applications: A review. *Current Applied Physics*, 16(9), p.1192-1201. https://doi.org/10.1016/j.cap.2016.03.026.

[7] Güçlü, A. D. and Potasz, P. and Hawrylak, P., **2013**. Zero-energy states of graphene triangular quantum dots in a magnetic field. *Physical Review B*, 88(15), p.155429. https://doi.org/10.1103/PhysRevB.88.155429.

[8] Tiutiunnyk, A. and Morales, A. L. and Bertel, R. and Restrepo, R. L. and Nava-Maldonado, F. M. and Martínez-Orozco, J. C. and Laroze, D. and Duque, C. A. and Correa, J. D. and Mora-Ramos, M. E., **2022**. Electronic, optical, and magnetic properties of doped triangular MoS_2 quantum dots: A density functional theory approach. *Physica Status Solidi B*, 259(3), p.2100509. https://doi.org/10.1002/pssb.202100509.

[9] Tiutiunnyk, A. and Laroze, D. and Correa, J. D. and Mora-Ramos, M. E., **2023**. Electronic and magnetic properties of stacked graphene quantum dots. *Diamond and Related Materials*, 131, p.109550. https://doi.org/10.1016/j.diamond.2022.109550.

[10] Tiutiunnyk, A. and Duque, C. A. and Caro-Lopera, F. J. and Mora-Ramos, M. E. and Correa, J. D., **2019**. Opto-electronic properties of twisted bilayer graphene quantum dots. *Physica E: Low-dimensional Systems and Nanostructures*, 112, p.36-43. https://doi.org/10.1016/j.physe.2019.03.028.

[11] Carr, S. and Massatt, D. and Fang, S. and Cazeaux, P. and Luskin, M. and Kaxiras, E., **2017**. Twistronics: Manipulating the electronic properties of two-dimensional layered structures through their twist angle. *Physical Review B*, 95(7), p.075420. https://doi.org/10.1103/PhysRevB.95.075420.

[12] Mogera, U. and Kulkarni, G. U., **2020**. A new twist in graphene research: Twisted graphene. *Carbon*, 156, p.470-492. https://doi.org/10.1016/j.carbon.2019.09.053.

[13] Dietrich, F. and Guevara, U. J. and Tiutiunnyk, A. and Laroze, D. and Cisternas, E., **2023**. Vacancies and Stone-Wales defects in twisted bilayer graphene: A comparative theoretical study. *FlatChem*, 41, p.100541. https://doi.org/10.1016/j.flatc.2023.100541.

[14] Tiutiunnyk, A. and Duque, C. A. and Caro-Lopera, F. J. and Mora-Ramos, M. E. and Correa, J. D., **2019**. Opto-electronic properties of twisted bilayer graphene quantum dots. *Physica E: Low-dimensional Systems and Nanostructures*, 112, p.36-43. https://doi.org/10.1016/j.physe.2019.03.028.

[15] Soler, J. M. and Artacho, E. and Gale, J. D. and García, A. and Junquera, J. and Ordejón, P. and Sánchez-Portal, D., **2002**. The SIESTA method for ab initio order-N materials simulation. *Journal of Physics: Condensed Matter*, 14(11), p.2745-2779. https://doi.org/10.1088/0953-8984/14/11/302.

© Ariston Publications 2026. All rights reserved.

[16] Artacho, E. and Anglada, E. and Diéguez, O. and Gale, J. D. and García, A. and Junquera, J. and Martin, R. M. and Ordejón, P. and Pruneda, J. M. and Sánchez-Portal, D. and Soler, J. M., **2008**. The SIESTA method; developments and applicability. *Journal of Physics: Condensed Matter*, 20(6), p.064208. https://doi.org/10.1088/0953-8984/20/6/064208.

[17] García, A. and Papior, N. R. and Akhtar, A. and Artacho, E. and Blum, V. and Bosoni, E. and Brandimarte, P. and others, **2020**. SIESTA: Recent developments and applications. *Journal of Chemical Physics*, 152(20), p.204108. https://doi.org/10.1063/5.0005077.

[18] Larsen, A. H. and Mortensen, J. J. and Blomqvist, J. and Castelli, I. E. and Christensen, R. and Dułak, M. and Friis, J. and Groves, M. N. and Hammer, B. and Hargus, C. and others, **2017**. The atomic simulation environment---A Python library for working with atoms. *Journal of Physics: Condensed Matter*, 29(27), p.273002. https://doi.org/10.1088/1361-648X/aa680e.

[19] Dion, M. and Rydberg, H. and Schröder, E. and Langreth, D. C. and Lundqvist, B. I., **2004**. Van der Waals density functional for general geometries. *Physical Review Letters*, 92(24), p.246401. https://doi.org/10.1103/PhysRevLett.92.246401.

ARISTON PUBLICATIONS

 © Ariston Publications 2026. All rights reserved.